Residual Strain Measurements in Thermal Spray Cermet Coatings via Neutron Diffraction

R. Ahmed[1]
e-mail: r.ahmed@hw.ac.uk

H. Yu

S. Stewart

School of Engineering and Physical Sciences,
Heriot-Watt University,
Edinburgh, EH14 4AS, UK

L. Edwards
Department of Materials Engineering,
The Open University,
Walton Hall,
Milton Keynes, MK7 6AA, UK

J. R. Santisteban
Rutherford Appleton Laboratory,
ISIS,
Didcot, OX11 0QX, UK

The impact and fatigue resistance of overlay coatings is significantly influenced by the residual strain (or stress) field induced during coating deposition, post-treatment, and in-service loading. Optimization of the residual strain field is therefore critical to the life and performance of components. Nondestructive measurement of these strain fields in relatively thin (300–400 μm) *thermal spray coatings, however, poses a challenge because conventional techniques, such as deep hole drilling, x-ray diffraction, synchrotron diffraction, and changes in beam curvature either make these techniques destructive and/or provides only a very near-surface strain measurement. This particularly complicates the strain analysis in cermet coatings, e.g.,* WC-Co *deposited by the thermal spraying process, where the low penetration depth of x-ray and synchrotron-diffraction ray can only provide a through thickness measurement of stress or strain profile via the destructive layer removal technique. Recent investigations have therefore concentrated on the use of neutron diffraction technique for such analysis, and this paper reports some of the early findings of the comparison of through thickness strain measurements in relatively thin* (400 μm) *as-sprayed and post-treated* WC-12wt. %Co *coatings via the neutron diffraction technique. Since neutrons are not charged, they do not interact with the electron cloud surrounding the atom (unlike x-ray); hence, diffraction results from the interaction with the atomic nucleus. Neutrons therefore have greater penetration depth in most engineering materials, and therefore provide a nondestructive through thickness strain measurement. Results of strain measurement are discussed with the structure property relationships and contact fatigue performance, and indicate that post-treatment of these coatings results in harmonization of the strain field within the coating, and at the coating substrate interface. This significantly influences the contact fatigue performance by improving both the cohesive and adhesive strength of these coatings.*
[DOI: 10.1115/1.2647503]

Keywords: neutron diffraction, residual stress, thermal spray coatings, rolling contact fatigue

1 Introduction

Thermal spraying is an overlay coating process in which molten or semi-molten coating powder particles are accelerated toward a substrate to form a coating. Tribological applications of thermally sprayed cermet coatings, e.g., those deposited by the high velocity oxy-fuel (HVOF) process, have greatly benefited from the recent advancements in thermal spray coating technology, e.g., higher impact velocity, and lower temperature and dwell time of the impacting lamellas. Excellent corrosive [1], erosive [2], abrasive [3], and fatigue/impact [4] resistance of these coatings (e.g., WC-Co, WC-Co-Cr) have resulted in environmentally friendly solutions for a range of engineering problems in automotive, aerospace, marine, and manufacturing industries. While industrial demands push the use of thermal spray cermet coatings toward high stress impact and fatigue resistance applications, the durability and safety implications dictate that these coatings should resist delamination and spalling failure under severe tribological conditions. A major factor dictating the resistance to fatigue and delamination failure in thermal spray coatings is the residual strain or stress field within the coating and substrate material.

There are a number of factors that dictate the overall residual stress profile in thermally sprayed deposits, as summarized in Fig. 1. Among them, the quenching (microtensile) residual stresses at the splat level due to the very high cooling rates (e.g., 1000 K/ms), and also macrocompressive or tensile residual stresses due to the mismatch of the coefficient of thermal expansion of the coating and substrate material play a dominant role. Very high impact velocity of lamella in the latest HVOF systems is also thought to improve residual stress or strain profile via penning effect. The influence of coating powder characteristics, coating process, and coating process parameters on the residual stress field has been the topic of research of many investigations [5–14] where experimental, mathematical, and numerical approaches have been adapted to ascertain the generation of residual stress during coating deposition. However, the investigations relating to the nondestructive measurement of residual stress/strain profile and the influence of post-treatments on these profiles for relatively thin (400 μm) cermet coatings have been limited. This is mainly because the penetration depth of x-ray and high-energy synchrotron radiations [15] is limited to few microns in WC-cermet coatings, making layer removal compulsory for depth profiling of residual strain. Although very near surface strain measurements by techniques such as x-ray diffraction and synchrotron diffraction are critical for durability studies of low stress components (e.g., in sliding wear), the catastrophic failures, such as delamination, either within the coating material or at the coating substrate interface, are dictated by the through thickness residual

[1]Corresponding author.

Contributed by the Tribology Division of ASME for publication in the JOURNAL OF TRIBOLOGY. Manuscript received March 15, 2006; final manuscript received January 9, 2007. Review conducted by Hong Liang. Paper presented at the STLE/ASME 2006 International Joint Tribology Conference (IJTC2006), San Antonio, Texas, USA, October 22–25, 2006.

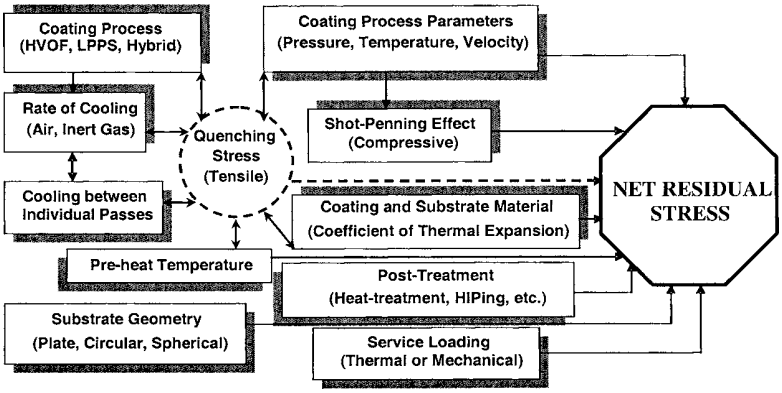

Fig. 1 Factors influencing the generation of residual stress in thermal spray coatings

strain profile. The destructive nature of these conventional techniques also limits their use in finished components, e.g., in aerospace applications.

Because of the difficulties in the nondestructive residual strain (or stress) profiling of these coatings, there has been a growing interest in the use of the neutron-diffraction technique [16–22], which has been applied to measure residual stress profile in thermal barrier coatings (TBCs) of zirconia, NiCrAlY, and yttria stabilized zirconia. These investigations have provided valuable information about the stress gradients, theoretical modeling of stress generation, and their influence on coating performance for relatively thick (typically, 1000 μm thick) thermal spray coatings. However, studies relating to the residual stress or strain changes through the post-treatment of thin (400 μm) cermet coatings have been limited. This investigation therefore aims to provide nondestructive strain measurement in thin cermet WC-12wt. %Co coatings in as-sprayed and post-treated conditions and relate it to the contact fatigue performance.

2 Experimental Test Procedure

2.1 Coating Preparation and Post-Treatment. Thermal spray HVOF (JP5000) WC-12wt. %Co coatings were deposited under industrially optimized conditions summarized in Table 1. Agglomerated and sintered powder with a size range of 15–45 μm was used for spraying the test coupons. These coatings were deposited on the surface of 32 mm dia and 8 mm thick (AISI 440-C) steel disks in two different thicknesses of 400 μm and 50 μm. The selection of substrate was based on its ability to support coating during impact and fatigue tests [4]. Coating thickness was varied to investigate both the cohesive and adhesive failures in contact fatigue tests. The coated specimens were also post-treated using un-encapsulated hot isostaic pressing (HIPing) for 1 h at a temperature and pressure of 1200°C and 103 MPa, respectively. These HIPing conditions were adapted on the basis of ongoing investigations of HIPing post-treatment on WC-cermet coatings [15,23–25].

Table 1 Deposition conditions for HVOF spraying

Coating type	WC-12wt. %Co, agglom. and sintered powder
Process/System	HVOF/ JP5000
Oxygen flow (l/min)	893
Kerosene flow (l/min)	0.32
Spraying distance (mm)	380
Spraying rate (g/min)	70

2.2 Powder and Coating Characterization. The surface and cross sections of coated specimens were investigated via scanning electron microscopy (SEM) equipped with energy dispersive x-ray spectroscopy (EDX). The x-ray diffraction (XRD) analysis of coatings was made using a Siemens D500 diffractometer with Cu-Kα source (1.5406 Å wavelength, step size of 0.02 deg, and dwell time of 2 s). Microhardness measurements were carried out under a load of 2.94 N using a Vickers microhardness (Mitutoyo-MVK-H1) test machine.

Elastic modulus measurements were performed via the indentation method. The indentation modulus was measured using the real-time force displacement curve under a load of 500 mN and correlated to the Young's modulus (E) using

$$E = Y_{HU}(1 - \nu^2) \tag{1}$$

where Y_{HU} is the indentation modulus and ν is the Poisson's ratio. Further details of this test method can be found in Buchmann et al. [26].

2.3 Neutron Diffraction Measurements. Neutron diffraction measurements were performed at ISIS (Rutherford Laboratory), UK using a dedicated strain measurement diffractometer (ENGIN). This is a pulsed neutron diffractometer equipped with slits and collimators to achieve small gage volumes [27,28]. This instrument operates in a fundamentally different manner from most reactor-based instruments, as instead of measuring Bragg reflections by scanning a detector from low to high 2θ, ENGIN, uses a pulsed polychromatic beam to measure Bragg reflections at fixed scattering angles (2θ=90 deg) using the time of flight of each diffracted neutron to characterize its wavelength [29,30].

Two different neutron diffraction configurations, i.e., horizontal scan (Fig. 2) and vertical scan (Fig. 3), can be applied for strain measurement in these coatings. The former configuration has previously been applied at ISIS [17], and by others (e.g., [18,20,21]), where neutron beam illuminates the coating surface at 45 deg, and the diffracted beam analyzed either in the reflection or transmission mode (Fig. 2). In this configuration, the in-plane stress is calculated by comparing the in-plane strain to the strain perpendicular to the plane, under the assumption of zero stress perpendicular to the plane of deposited layers. However, this configuration can incorporate pseudo-strains [31], which can be very large, often bigger than the physical strain in the component surface, and conventionally can only be dealt with either with a specific calibration measurement [18] or Monte-Carlo-type simulation of each measurement geometry used. Furthermore, the magnitude of the effect is unique to each specimen and diffractometer used. This technique, as just noted, can produce inevitable systematic errors which manifest as pseudostrains because the "sample gage volume," i.e., the intersection of the instrumental gage volume (black

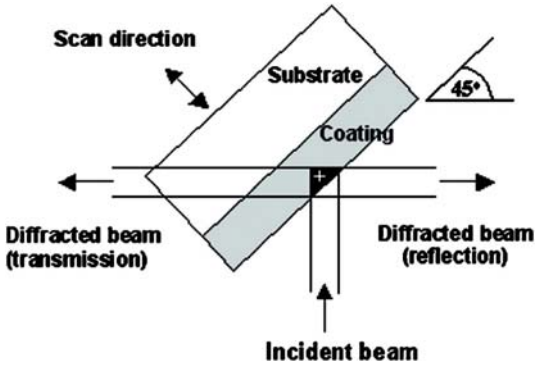

Fig. 2 Horizontal scan of the coated sample relative to the fixed gage volume in reflection and transmission mode to measure strain. Cross indicates the center of gravity of gage volume.

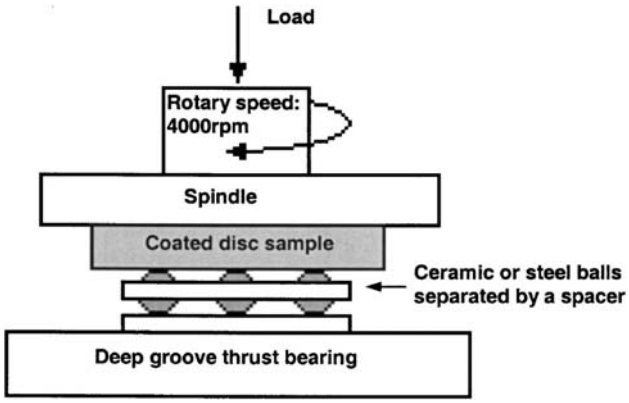

Fig. 4 Schematic illustration of the cup assembly for rolling contact fatigue tests

squares in Fig. 2) with the sample changes through the scan.

However, if the incident beam is scanned vertically out of a horizontal surface as shown in Fig. 3, there is no change in the diffraction angle and, hence, no pseudo strains generated as the gage volume moves out of the surface [29]. In the present work, this "vertical scan" arrangement was therefore adopted. The coated specimen was moved up or down in the z direction for the depth profiling of strain in the coating and substrate material. The incident beam was passed through a vertical and horizontal slit assembly to give a beam height at the slits of 0.3 mm. However, because of beam divergence (Penumbra effects), the maximum extent of the gage volume was $0.5\times0.5\times10$ mm^3. Partially submerging the gage volume allowed the strain in the coated material to be measured, whereas the substrate strain was mostly measured using a fully submerged gage volume. Longer measurement times were therefore required for the strain measurement in the coating material. The center of gravity of the gage volume was used to measure the depth of strain measurement.

Strains were computed from the diffraction data using two different techniques of "Pawley refinement" and the shift in individual WC (101) peaks for the substrate and coating materials, respectively [32–34]. Pawley refinement, unlike individual peak shift method, considers the entire spectrum. Pawley refinement could however not be applied to measure strain in the post-treated coating, as the diffraction pattern was too complicated for Pawley refinement (as shown later), and individual peak shifts for the coating materials were used for the comparative analysis of the as-sprayed and post-treated coatings. WC-101 peak was selected for the strain analysis within the coating material, as this peak had none or minimum overlap with other peaks, either due to the presence of complex WC- or substrate-phases, when gage volume was located within the two materials.

Residual strain (ε) values were calculated using the shift in the diffraction peak using

$$\varepsilon = \frac{d - d_0}{d_0} \tag{2}$$

where d and d_0 were the measured and strain-free lattice parameters, respectively. Residual strain values were then related to the residual stress values using the modulus data (Eq. (1)). The strain-free lattice parameter (d_0) for the as-sprayed and posttreated coating material was obtained by carefully removing the coating from the substrate and crushing the deposit to form a powder. This powder was then put in a vanadium tube and its diffraction measured using a neutron beam of dimensions $4\times4\times4$ mm^3. Although a straightforward measurement of the agglomerated and sintered coating powder prior to spraying would have been easier, this technique was adapted to avoid any changes in the lattice parameters due to metallurgical changes during the thermal spraying process. The strain-free lattice parameter (d_0) for the steel substrate was evaluated by very near-surface measurement on the surface of steel disk.

2.4 Rolling Contact Fatigue (RCF) Tests. In order to ascertain the delamination and fatigue resistance of thermal spray coatings, coated specimens were subjected to rolling contact fatigue (RCF) tests. A modified four ball machine (TE92-HS) was used to study the RCF performance of the as-sprayed and HIPed thermal

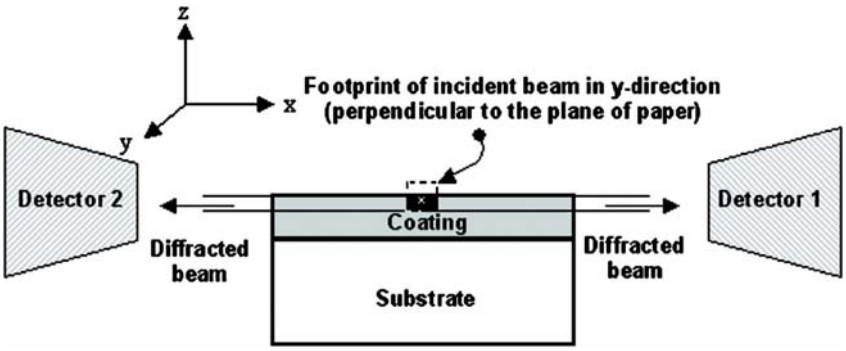

Fig. 3 Vertical (z) scan used for neutron diffraction measurements for in-plane strain. 2θ is fixed at 90 deg for both detectors. Strain is averaged from the two detectors. Cross indicates the center of gravity of gauge volume

spray rolling elements, as shown schematically in Fig. 4. In this setup, the coated disk was assembled to the drive shaft via a collet and drove three planetary balls, which acted as the thrust rolling elements in the configuration of a deep groove ball bearing. These tests were conducted in both steel and hybrid ceramic configurations, by replacing the steel balls with silicon nitride ceramic. RCF tests were conducted under immersed lubrication conditions, using Vitrea 320 oil at a spindle speed of 4000 ± 10 rpm, at two stress levels of 2 GPa and 2.7 GPa. The half contact width a approximated from Hertzian stress field was approximated in the range of 130–170 μm for the contact loads and configurations used in the test assembly. Failure was defined as the increase in vibration amplitude above a preset level. The ratio λ of the elastohydrodynamic lubricant (EHL) film thickness to the average surface roughness was calculated as $\lambda > 3$ under the given test conditions. Further details of the test method and ball kinematics can be appreciated from Stewart et al. [23] and Stewart and Ahmed [24].

3 Results

3.1 Coating Microstructure. Figure 5 shows the SEM observations of the 400 μm thick coating microstructure in the as-sprayed and post-treated conditions. Figure 5(*a*) shows the typical lamella morphology of the as-sprayed microstructure. Figure 5(*b*) shows the comparative carbide morphology after the HIPing post-treatment at a higher magnification. Figure 5(*c*) shows the formation of diffusion layer at the coating substrate interface after the post-treatment. The thickness of this diffusion later was approximately 13–15 μm. Figure 6 shows the XRD pattern of both the as-sprayed and post-treated coatings and indicate the presence of eta-phases (Co_6W_6C, Co_3W_3C) after the post-treatment. Figure 7 shows the neutron diffraction pattern obtained at the location of newly formed diffusion layer after the HIPing post-treatment. This diffraction pattern also include the Fe-α reflections from the substrate, and WC reflections from within the coating layer, as the gage volume was located within the top coating layer, diffusion zone, and the substrate material. Such analysis is not currently possible nondestructively using the conventional x-ray technique, and provides useful microstructural information, e.g., the formation of Fe_3W_3C after the HIPing post-treatment, which shows crystallographic phases of the solid solution after diffusion across the coating substrate interface. The microstructure and diffraction pattern of relatively thinner 50 μm coatings was similar to the 400 μm coatings.

3.2 Hardness and Indentation Modulus Measurements. Figure 8 shows the through thickness indentation hardness and indentation modulus measurements of the as-sprayed and HIPed coatings. These measurements indicate an increase in the hardness and modulus of coatings after the post-treatment. Generally, thermal spray coatings are expected to have anisotropic microstructure; however, indentation modulus measurements indicate negligible changes along and across the coating surface.

3.3 Residual Strain Via Neutron Diffraction. Figure 9 summarize the residual stress and strain measurement results for the 400 μm thick coatings. Because of very small ratio of coating to substrate thickness, the depth is shown in log scale. These measurements indicate significantly large values of as-sprayed coating strain, in comparison to the HIPed coatings, and also highlight the differences in the strain profile at the coating substrate interface.

3.4 RCF Results. Figure 10 summarizes the test configuration, stress level, and relative RCF performance comparison of the as-sprayed and HIPed coatings. It is to be appreciated that these results are not intended for the statistical fatigue prediction, but to comprehend the relative performance and failure modes of the as-sprayed and HIPed coatings. Test results indicate that for both stress levels (2 GPa and 2.7 GPa) and both test configurations (conventional steel and hybrid ceramic), the relative performance

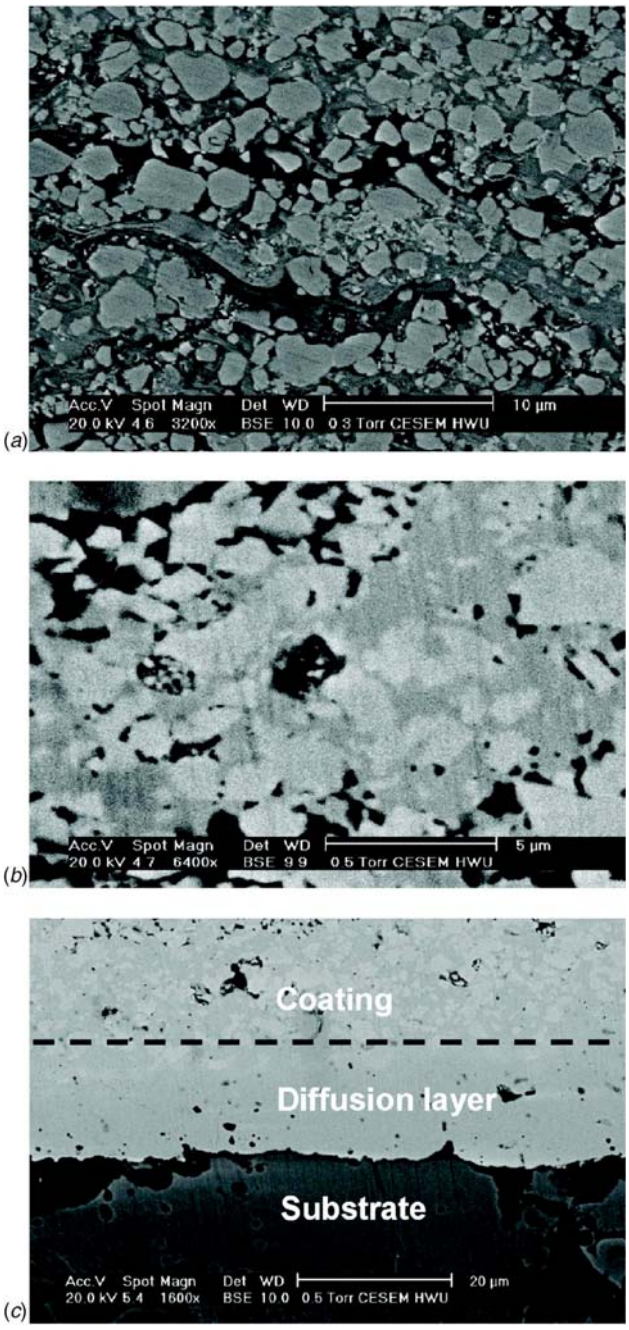

Fig. 5 Microstructure of 400 μm thick coatings: (a) as-sprayed coating, (b) HIPed coating, and (c) coating/substrate interface after HIPing

of coatings improved after the HIPing post-treatment. Typical SEM observations of the failed areas of the as-sprayed and HIPed coatings are shown in Figs. 11 and 12 for the 400 μm and 50 μm thick coatings, respectively. Failure mode of these coatings varied as spalling, macropitting, and delamination, depending on the contact configuration, load, and coating thickness. A three-dimensional white light interferometer (Zygo-New View) was used to measure the depth of coating failure. For the case of 400 μm thick coatings, the failure depth varied from 13 μm to 25 μm, whereas for the case of relatively thin 50 μm thick coat-

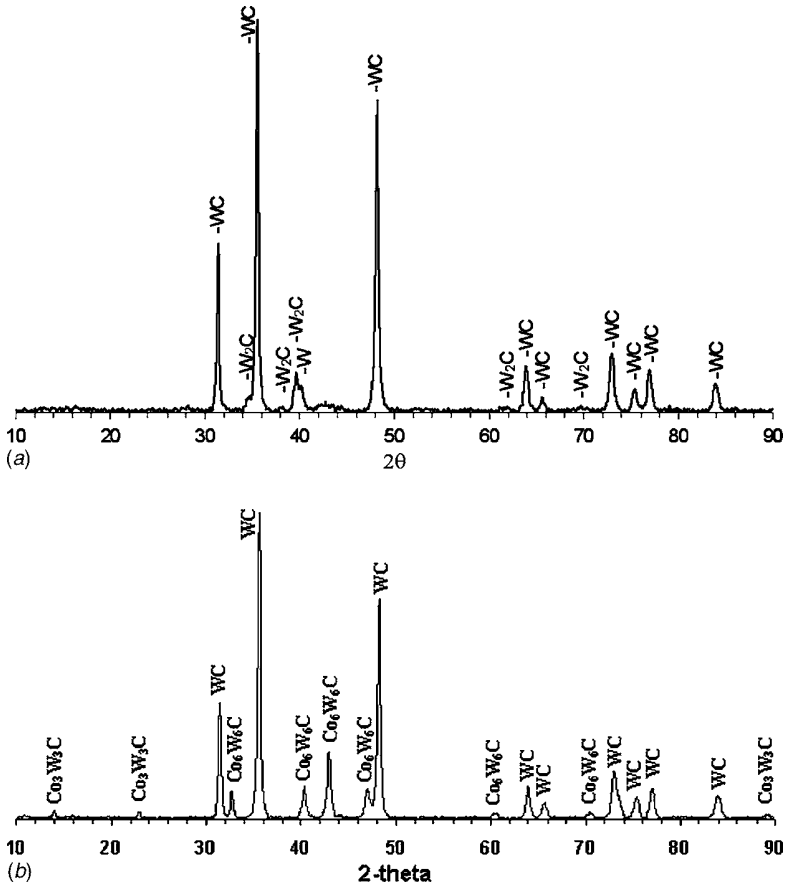

Fig. 6 XRD pattern of the coatings: (a) as-sprayed coating and (b) HIPed coating

ings, the failure depths were measured in the range of 14 μm to 50 μm for the various test conditions adapted in this investigation.

4 Discussion

4.1 Coating Microstructure. The lamellar microstructure of thermal spray coatings has been a topic of research for a number of investigations [e.g., [35–37]] and has provided useful information on the influence of coating powder characteristics, coating process, and process conditions on the resulting microstructure. The XRD pattern of the as-sprayed coating shown in Fig. 6 indicate some carburization, which results in the transformation of some WC into W_2C and W. The mechanisms of these transformations are well understood on the basis of carbon loss either as CO_2 and/or nanocrystalline phases [35–37]. The aim of the discussion here is therefore to consider the microstructural changes caused by the HIPing post-treatment and relate them to the tribomechanical investigations. The XRD analysis of the post-treated coatings (Fig. 6(*b*)) indicate two major transformations. First, the formation of η-phases (Co_6W_6C and Co_3W_3C) by the interaction of matrix (Co) and carbide (WC) at their interfacial boundary within

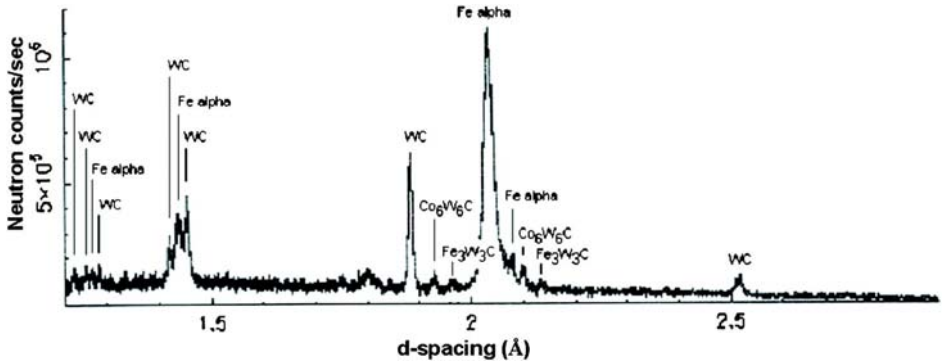

Fig. 7 Neutron diffraction pattern of the 20 μm diffusion layer formed at the coating/substrate interface after the HIPing post-treatment

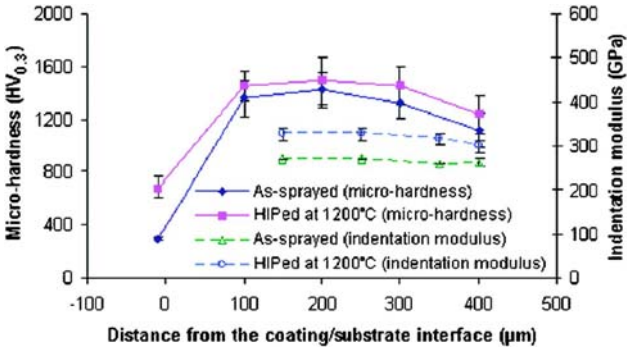

Fig. 8 Hardness and indentation modulus measurement results for the as-sprayed and HIPed coatings

the coating microstructure. Second, the elimination of W_2C and W to form η-phases and/or solid solution after their interaction with the matrix (Co). The former transformation resulted from the dissolution of WC grains at their boundary with the cobalt matrix, whereas the latter was a result of the crystallization of amorphous phases and dissolution of W_2C and W in the metal binder. These changes during the post-treatment were underpinned by the changes in the inter-splat bonding mechanism from mechanical interlock to metallurgical bonding, as indicated by the XRD and SEM observations, and confirmed by the modulus measurements.

At the coating substrate interface, the diffusion of Fe from the substrate toward the coating, and Co from the coating into the substrate, results in the formation of a diffusion layer, as shown in Fig. 5(*c*). The neutron diffraction pattern (Fig. 7) of this diffusion

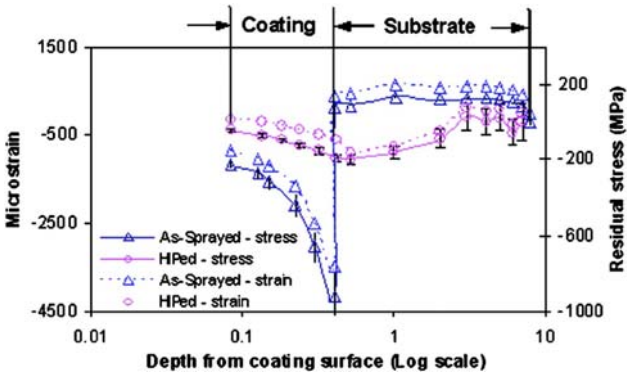

Fig. 9 Vertical scan results comparing microstrain and residual stress in 0.4 mm thick WC-Co coatings in the as-sprayed and HIPed conditions

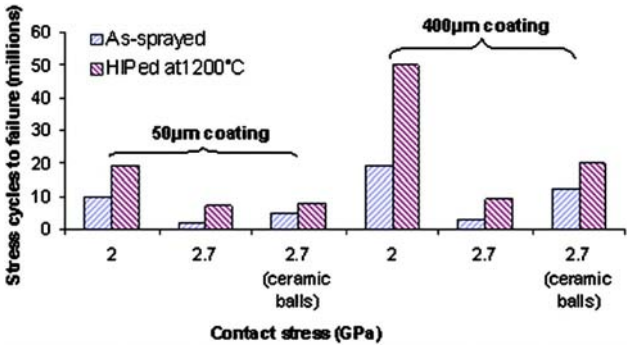

Fig. 10 RCF test results for the as-sprayed and HIPed coatings in steel and ceramic ball configurations

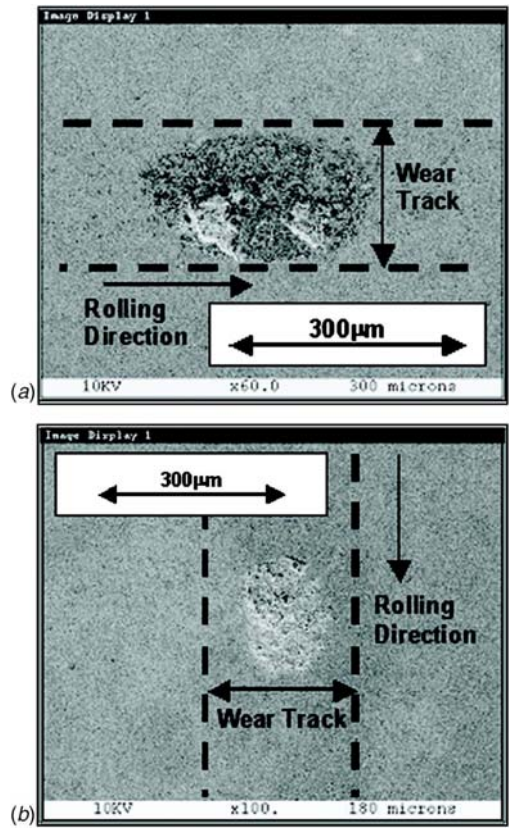

Fig. 11 Surface observations of 400 μm thick coatings subjected to 2.7 GPa contact stress using conventional steel ball contact configuration: (a) spalling in the as sprayed coating and (b) macropitting in the HIPed coating

layer indicates the formation of Fe_3W_3C, which was not seen in the top coating layer (see Fig. 6), indicating carbide dissolution (Fig. 5(*c*)) and formation of solid solution within the diffusion zone. These mechanisms of diffusion have previously been confirmed and discussed by the author(s) using the EPMA maps of elemental species of HIPed WC-Co coatings, further details of which can be appreciated from Tobe et al. [38]. The formation of this diffusion zone therefore indicates that, in addition to the changes in the intersplat bonding mechanism outlined above, the coating substrate interface is further strengthened by the metallurgical bonding due to the diffusion of species. The former therefore improves the cohesive strength of the coating, whereas the latter results in improving the adhesive strength of the coating. Both of these factors significantly influence coating's tribomechanical performance as discussed next.

4.2 Hardness and Modulus Measurements. Coating hardness increased after the HIPing post-treatment, which was mainly due to the formation of harder η-phases within the coating microstructure (Fig. 6). This was consistent with previous studies on the post-treatment of thermal spray coatings [e.g., [37–39]]. These changes were seen not only on the coating surface but also throughout the coating section. The diffusion of elemental species at the coating substrate interface also resulted in the changes in the substrate hardness near this interface. The formation of η-phases, should, in principle, also increase the brittleness within the coating microstructure. However, in this case this expected increase was offset by the changes in the bonding mechanisms within the coating microstructure, resulting in the higher modulus of the post-treated coatings (Fig. 8). Although qualitative toughness measurements have not been shown here, previous investiga-

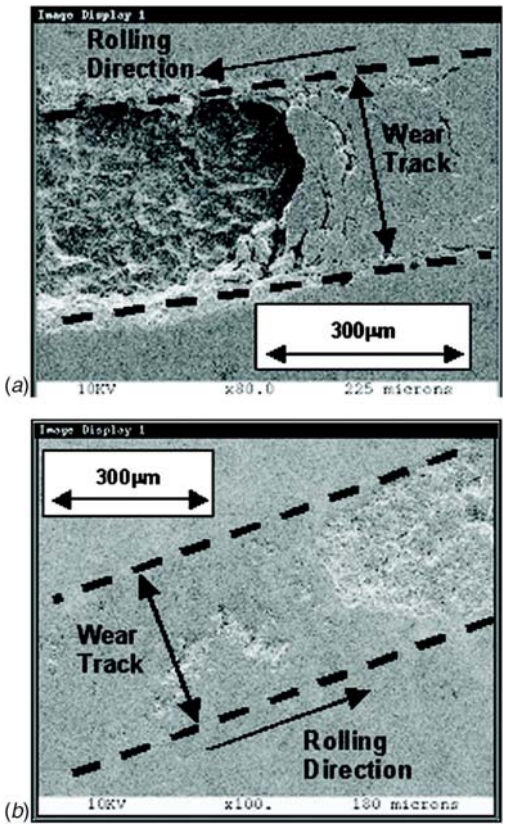

Fig. 12 Surface observations of 50 μm thick coatings subjected to 2.7 GPa contact stress using conventional steel ball contact configuration: (a) delamination in the as sprayed coating and (b) surface pitting in the HIPed coating

tions by the author(s) have shown that these changes in the coating microstructure and modulus are associated with improvement in coating toughness [25].

4.3 Residual Strain Measurements. The residual strain/stress measurements shown in Fig. 9 indicate compressive values in the coating material for both the as-sprayed and HIPed conditions. This was mainly because of the relatively higher coefficient of thermal expansion of the substrate material, and consistent with previous studies on WC-Co coatings (e.g., [9,11]). The strain gradient was however much steeper for the as-sprayed coating, indicating a high through thickness strain variation in comparison to the HIPed coating. These variations were caused by the rapid cooling of the deposit during spraying. The values of compressive strain in the as-sprayed coating were therefore much higher than the HIPed coating, which can significantly influence the impact and fatigue resistance by acting as stress concentrations. Although a certain degree of compressive residual stress is always beneficial for the fatigue and impact resistance of these coatings, very high compressive stress (or strain) as seen in this case can have detrimental effects, and thus need to be carefully controlled during coating deposition and/or subsequent post-treatment. The diffusion zone formed during the HIPing post-treatment (Fig. 5(*c*)), also had a significant influence on the coating substrate interfacial strain. It can be appreciated that at the coating substrate interface, there is a rather large shift in the residual strain profile of the as-sprayed coating, which was caused by the mismatch of the thermal and mechanical properties of the coating and substrate material. However, for the case of HIPed coating, there is a uniform transition of strain at the coating substrate interface, thereby minimizing the stress concentrations at this location. These differences in the strain pattern of the as-sprayed and HIPed coatings had a significant effect on the contact fatigue performance.

4.4 RCF Performance and Failure Modes

4.4.1 400 μ*m Thick Coatings*. Previous studies on the RCF performance and failure modes of thermal spray coatings have indicated that for the case of relatively thick coatings (coating thickness >200 μm), the failure is generally within the coating material [40,41]. These cohesive failures result from the orthogonal and maximum shear stress due to contact loading, which are located within the coating material, well above the coating substrate interface. In the current set-up of contact load and coating thickness, these depths were approximately in the range of 45–87 μm. Cohesive failures were therefore seen in all the cases of 400 μm thick coatings, as confirmed by the SEM observations presented in Fig. 11. The depth of failures in these coatings was approximated in the range of 13–25 μm. This is typical of RCF failure modes in thermal spray coatings, where although subsurface cracks initiate at the location of orthogonal and maximum shear stress, the failure is generally at a shallower depth, due to the changes in crack directions and interaction of a number of microcracks, which become unstable at shallower depths. Further details of these failure modes in thermal spray cermet coatings can be appreciated elsewhere [40,41]. The residual stress gradient within the coating was therefore critical to the RCF performance, as these stresses were superimposed on the Hertzian stress field. High values of residual strain (or stress) and its sharp gradient therefore significantly influenced the impact and fatigue performance. Changes in the coating bonding mechanism from the mechanical interlock to metallurgical bonding, as confirmed by the modulus measurements, coupled with the homogenization and reduction of residual strain gradient after the HIPing post-treatment, therefore improved the cohesive strength of the coating. Both of these factors were therefore critical in improving the RCF performance of 400 μm thick coatings after the HIPing post-treatment.

4.4.2 50 μ*m-Thick-Coatings*. When the coatings were relatively thin, the maximum shear stress and orthogonal shear stress were located near the coating substrate interface. These coatings therefore delaminated and/or spalled at this interface, as shown in Fig. 12, which was further confirmed by the depth of failures (14–50 μm). The failure mode in these coatings was generally catastrophic delamination at or near the coating-substrate interface, due to poor adhesive strength, especially for the case of as-sprayed coatings. Although improvement in coating's cohesive strength after the HIPing post-treatment did play a part in resisting delamination failure, it was the adhesive strength of the coating that dictated the fatigue and impact performance of these relatively thin (50 μm) coatings.

Considering the role of changes in the residual stress/strain profile for the 50 μm coatings after the HIPing post-treatment, and its influence on the RCF performance, it can be appreciated that the residual strain profile at the coating substrate will change due to the formation of diffusion zone. Although, the through thickness residual strain results for the 50 μm thick coatings are not included here, it can be appreciated that a similar homogenization of strain field at the coating substrate interface will occur after the HIPing post-treatment, as was observed for the 400 μm thick coatings, since it was a function of the formation of diffusion zone at the interface. Formation of diffusion zone was therefore critical in improving the adhesive strength of coatings, and thus resulted in relatively improved RCF performance of the HIPed 50 μm coatings (Fig. 10).

5 Conclusions

1. Vertical scanning technique has been successfully applied to measure the residual strain via neutron diffraction in 400 μm thick WC-Co thermal spray coatings.

2. Significant improvements in the RCF performance were observed after the HIPing post-treatment for both the 400 μm and 50 μm thick coatings. These improvements were caused by the respective increase in the cohesive and adhesive strength of the coated layer due to the changes in the residual strain profile, and metallurgical bonding at the intersplat and coating substrate interface level.
3. HIPing post-treatment reduces the residual strain gradient within the coating layer, and also homogenizes the strain profile by minimizing the stress gradient at the coating substrate interface.
4. Indentation modulus measurements indicate improvements in the bonding mechanisms (cohesive strength) after the HIPing post-treatment.
5. Formation of diffusion zone at the coating substrate interface resulted in improved adhesive strength as indicated by the RCF performance of relatively thinner (50 μm thick) coatings.

References

[1] Daniel, R. L., Sanders, H. L., and Mendrek, M. J., 1994, "Replacement of Environmentally Hazardous Corrosion Protection Paints on the Space Shuttle Main Engine Using Wire Arc Sprayed Aluminium," *Proc. of 7th National Thermal Spray Conference*, Boston, ASM International, Materials Park, OH, pp. 93–98.

[2] Rhys-Jones, T. N., 1990, "The Use of Thermally Sprayed Coatings for Compressor and Turbine Applications in Aero-Engines," Surf. Coat. Technol., **42**, pp. 1–11.

[3] Chen, H., and Hutchings, I. M., 1998, "Abrasive Wear Resistance of Plasma-Sprayed Tungsten Carbide Cobalt Coatings," Surf. Coat. Technol., **107**(2–3), pp. 106–114.

[4] Osawa, S., Itsukaichi, T., and Ahmed, R., 2005, "Influence of Substrate Properties on the Impact Resistance of WC Cermet Coatings," J. Therm. Spray Technol., **14**(4), pp. 495–501.

[5] Greving, D. J., Rybicki, E. F., and Shadley, J. R., 1994, "Through-Thickness Residual Stress Evaluations for Several Industrial Thermal Spray Coatings Using a Modified Layer-Removal Method," J. Therm. Spray Technol., **3**(4), pp. 379–388.

[6] Gassot, H., Junquera, T., Jeandin, V. J. M., Guipont, V., Coddet, C., Varney, C., and Grandsire, L., 2001, "Comparative Study of Mechanical Properties and Residual Stress Distributions of Copper Coatings Obtained by Different Thermal Spray Processes," Surf. Eng., **17**(4), pp. 317–322.

[7] McGrann, R. T. R., Greving, D. J., Shadley, J. R., Rybicki, E. F., Bodger, B. E., and Somerville, D. A., 1998, "Effect of Residual Stress in HVOF Tungsten Carbide Coatings on the Fatigue Life in Bending of Thermal Spray Coated Aluminum," J. Therm. Spray Technol., **7**(4), pp. 546–552.

[8] Matejicek, J., Sampath, S., and Dubsky, J., 1998, "X-Ray Residual Stress Measurements in Metallic and Ceramic Plasma Sprayed Coatings," J. Therm. Spray Technol., **7**(4), pp. 489–496.

[9] Stokes, J., and Looney, L., 2004, "Residual Stress in HVOF Thermally Sprayed Thick Deposits," Surf. Coat. Technol., **177-178**, pp. 18–23.

[10] Buchmann, M., Gadow, R., and Tabellion, J., 2000, "Experimental and Numerical Residual Stress Analysis of Layer Coated Composites," Mater. Sci. Eng., A, **288**, pp. 154–159.

[11] Ahmed, R., and Hadfield, M., 1997, "Experimental Measurement of the Residual Stress Field within Thermally Sprayed Rolling Elements," Wear, **209**, pp. 84–95.

[12] McGrann, R. T. R., Greving, D. J., Shadley, J. R., Rybicki, E. F., Kruecke, T. L., and Bodger, B. E., 1998, "The Effect of Residual Stress on the Fatigue Life of Thermal Spray-Coated Steel and Aluminum," Surf. Coat. Technol., **108-109**, pp. 59–64.

[13] Gill, S. C., 1993, "Residual Stress in Plasma Sprayed Deposits," Ph.D. thesis, Gonville and Caius College, Cambridge University, UK.

[14] Matejicek, J., 1999, "Processing Effects on Residual Stress and Related Properties of Thermally Sprayed Coatings," Ph.D. thesis, Materials Science and Engineering, State University of New York, Stony Brook.

[15] Stoica, V., Ahmed, R., Golshan, M., and Tobe, S., 2004, "Sliding Wear Evaluation of Hot Isostatically Pressed (HIPed) Thermal Spray Cermet Coatings," J. Therm. Spray Technol., **13**(1), pp. 93–107.

[16] Kesler, O., Matejicek, J., Sampath, S., Suresh, S., Gnaeupel-Herold, T., Brand, P. C., and Prask, H. J., 1998, "Measurement of Residual Stress in Plasma-Sprayed Metallic, Ceramic and Composite Coatings," Mater. Sci. Eng., A, **257**, pp. 215–224.

[17] Scardi, P., Leoni, M., Bertini, L., Bertamini, L., and Crenuschi, F., 1998, "Strain Gradients in Plasma-Sprayed Zirconia Thermal Barrier Coatings," Surf. Coat. Technol., **108-109**, pp. 93–98.

[18] Matejicek, J., Sampath, S., Brand, P. C., and Prask, H. J., 1999, "Quenching, Thermal and Residual Stress in Plasma Sprayed Deposits: NiCrAlY and YSZ Coatings," Acta Mater., **47**(2), pp. 607–617.

[19] Turquier, F., Ceretti, M., Hairy, P., Titeux, I., and Lodini, A., 2000, "Residual Stress Measurements in a Tool Steel Coated with Plasma-Sprayed Zirconia and Submitted to Thermal Fatigue in Liquid Aluminium," Physica B, **276-278**, pp. 872–873.

[20] Keller, T., Margadant, N., Pirling, T., Escribano, M. J. R., and Wagner, W., 2004, "Residual Stress Determination in Thermally Sprayed Metallic Deposits by Neutron Diffraction," Mater. Sci. Eng., A, **373**, pp. 33–44.

[21] Sampath, S., Jiang, X. Y., Matejicek, J., Prchlik, L., Kulkarni, A., and Viadya, A., 2004, "Role of Thermal Spray Processing Method on the Microstructure, Residual Stress and Properties of Coatings: An Integrated Study for Ni-5wt. %Al Bond Coats," Mater. Sci. Eng., A, **364**, pp. 216–23.

[22] Markocsan, N., Nylen, N., Fogarassy, P., and Manescu, A., 2004, "Residual Stress Analysis in Plasma Sprayed Free-Standing Zirconia Components," *Proc. of ITSC-2004*, Osaka, ASM International, Materials Park, OH, pp. 101–106.

[23] Stewart, S., Ahmed, R., and Itsukaichi, T., 2004, "Contact Fatigue Failure Evaluation of Post-Treated WC-NiCrBSi Functionally Graded Thermal Spray Coatings," Wear, **257**, pp. 962–983.

[24] Stewart, S., and Ahmed, R., 2003, "Contact Fatigue Failure Modes in Hot Isostatically Pressed WC-12%Co Coatings," Surf. Coat. Technol., **172**, pp. 204–216.

[25] Stoica, V., Ahmed, R., and Itsukaichi, T., 2005, "Influence of Heat Treatment on the Sliding Wear of Thermal Spray Cermet Coatings," Surf. Coat. Technol., **199**, pp. 7–21.

[26] Buchmann, M., Escribano, M., Gadow, R., and Burkle, G., 2002, "On the Elastic Mechanical Properties of Thermally Sprayed Coatings," *Thermal Spray: Surface Engineering via Applied Research*, C. C. Berndt, ed., ASM International, pp. 598–605.

[27] Allen, W., Andreani, C., Hutchings, M. T., and Windsor, C. G., 1985, "Neutron Diffraction Methods for the Study of Residual Stress Fields," Adv. Phys., **34**, pp. 445–473.

[28] Daymond, M. R., Bourke, M. A. M., Von Dreele, R. B., Clausen, B., and Lorentzen, T., 1997, "Use of Rietveld Refinement for Elastic Macrostrain Determination and for the Evaluation of Plastic Strain History From Diffraction Spectra," J. Appl. Phys., **82**, pp. 1554–1562.

[29] Fitzpatrick, M. E., and Lodini, A., 2003, *Analysis of Residual Stress by Diffraction using Neutron and Synchrotron Radiation*, Taylor & Francis, London.

[30] Hutchings, M. T., Withers, P. J., Holden, T. M., and Lorentzen, T., 2005, *Introduction to the Characterization of Residual Stress by Neutron Diffraction*, CRC Press, Taylor & Francis, Boca Raton.

[31] Johnson, M. W., Edwards, L., and Withers, P. J., 1997, "ENGIN - A New Instrument for Engineers," Physica B, **234**, pp. 1141–1143.

[32] Noyan, I. C., and Cohen, J. B., 1987, *Residual Stress*, Springer-Verlag, Berlin.

[33] Pawley, G. S., 1981, "Unit-Cell Refinement from Powder Diffraction Scans," J. Appl. Crystallogr., **14**, pp. 357–361.

[34] Withers, P. J., Johnson, M. W., and Wright, J. S., 2000, "Neutron Strain Scanning Using a Radially Collimated Diffracted Beam," Physica B, **292**, pp. 273–285.

[35] Lovelock, H., 1998, "Powder/Processing/Structure Relationships in WC-Co Thermal Spray Coatings: A Review of the Published Literature," J. Therm. Spray Technol., **7**(3), pp. 357–373.

[36] Verdon, C., Karimi, A., and Martin, J. L., 1998, "A Study of High Velocity Oxy-Fuel Thermally Sprayed Tungsten Carbide Coatings, Part 1: Microstructures," Mater. Sci. Eng., A, **246**, pp. 11–24.

[37] Nerz, J. E., Kushner, B. A., and Rotolico, A. J., 1992, "Microstructural Evaluation of Tungsten Carbide-Cobalt Coatings," J. Therm. Spray Technol., **1**(2), pp. 155–160.

[38] Tobe, S., Ando, Y., Ahmed, R., and Stoica, V., 2003, "Enhancement of Wear and Mechanical Properties of Thermally Sprayed WC-Co Coatings by HIPing Post-Treatment," *Proc. of Tribology in Environmental Design*, Bournemouth, UK, Professional Engineering Publishing Ltd., London, pp. 119–127.

[39] Ito, H., Nakamura, R., Shiroyoma, M., and Sasaki, T., 1990, "Post-Treatment of Plasma Sprayed WC-Co Coatings by Hot Isostatic Pressing," *Proc. of 3rd National Thermal Spray Conference*, Long Beach, CA, ASM International, Materials Park, OH, pp. 233–238.

[40] Ahmed, R., 2002, "Rolling Contact Fatigue," *ASM Handbook*, R. J. Shipley and W. T. Becker, eds., ASM International, 11(6E), pp. 941–956.

[41] Ahmed, R., and Hadfield, M., 2002, "Mechanisms of Fatigue Failure in Thermal Spray Coatings," J. Therm. Spray Technol., **11**(3), pp. 333–349.